Optical properties of charged quantum dots doped with a single magnetic impurity

U. C. Mendes,[1,2] M. Korkusinski,[1] A. H. Trojnar,[1,3] and P. Hawrylak[1,3]

[1]*Quantum Theory Group, Security and Disruptive Technologies, National Research Council, Ottawa, Canada K1A0R6*
[2]*Institute of Physics "Gleb Wataghin", State University of Campinas, Campinas-SP, Brazil*
[3]*Department of Physics, University of Ottawa, Ottawa, Canada*

We present a microscopic theory of the optical properties of self-assembled quantum dots doped with a single magnetic manganese (Mn) impurity and containing a controlled number of electrons. The single-particle electron and heavy-hole electronic shells are described by two-dimensional harmonic oscillators. The electron-electron, electron-hole Coulomb as well as the short-range electron spin-Mn spin and hole spin-Mn spin contact exchange interactions are included. The electronic states of the photoexcited electron-hole-Mn complex and of the final electron-Mn complex are expanded in a finite number of configurations and the full interacting Hamiltonian is diagonalized numerically. The emission spectrum is predicted as a function of photon energy for a given number of electrons and different number of confined electronic quantum dot shells. We show how emission spectra allow to identify the number of electronic shells, the number of electrons populating these shells and, most importantly, their spin. We show that electrons not interacting directly with the spin of Mn ion do so via electron-electron interactions. This indirect interaction is a strong effect even when Mn impurity is away from the quantum dot center.

I. INTRODUCTION

There is currently interest in developing means of controlling spin at the nanoscale.[1–7] This includes spin of electrons and holes in gated[8,9] and self-assembled quantum dots[10,11] as well as magnetic impurities in semiconductors.[5,6] It is now possible to place, optically detect, and manipulate a single magnetic impurity in a single self-assembled quantum dot (QD).[12–19] The electrical control of the spin of manganese (Mn) ions in CdTe quantum dots with a small electron population controlled by the gate has been implemented.[20] The properties of CdTe quantum dots with magnetic impurities have been extensively investigated theoretically,[1,18,21–29] including the theory of Coulomb blockade and capacitance spectroscopy,[21,24,30] cyclotron resonance,[27] and photoluminescence (PL).[18,22,26,31,32] The optical properties of carriers confined in III-V quantum wells[33] and quantum dots[15] containing Mn ions have also been investigated.

The electronic properties of quantum dots containing N_e electrons and a single localized spin have been investigated theoretically.[22,24] It was shown that the electron spin can be controlled by controlling the number N_e (see Refs. [24] and [31]). For closed electronic shells, the total spin is zero and electrons are decoupled from the Mn spin, while for half-filled shells the electron spin is maximized and the coupling to the Mn spin is strongest.[24,31] The spin-singlet N_e-electron droplet coupled to the Mn spin gives insight into the Kondo effect in the interacting electron system, and this coupling might potentially allow for direct detection of the electron spin. Simultaneously, the optical properties of charged QDs without magnetic ions have been studied both numerically and experimentally.[34–37]

Here we present a microscopic theory of the optical properties of charged self-assembled quantum dots doped with a single magnetic Mn ion as a function of number of electrons N_e. The single-particle electron and heavy-hole electronic shells are described by states of a two-dimensional harmonic oscillator. The electron-electron, electron-hole Coulomb interactions, as well as the short-range electron spin-Mn spin

and hole spin-Mn spin contact exchange interactions are included. The electronic states of the photoexcited $N_e + 1$ electron- 1 hole- 1 Mn complex ($X^{N_e-} + \text{Mn}$) and of the final N_e electron-Mn complex ($N_e + \text{Mn}$) are expanded in a finite number of configurations. The full interacting initial and final state Hamiltonians are diagonalized numerically. The emission spectra as a function of photon energy are obtained from Fermi's golden rule as a function of N_e. We show that the emission spectra depend on the number N_e, the position of Mn ion, the spin of the initial and final electronic states, and the size of the QD measured by the number of confined electronic shells. We demonstrate that the emission spectra allow to establish the number of electrons N_e populating electronic shells and, most importantly, to read the electronic spin through multiplets of energy levels manifested in the number of emission lines. If the Mn ion is placed in the center of the QD, the p-shell electrons do not interact with it directly. However, we show that in this case, there exists an effective electron-Mn interaction mediated by electron-electron interactions. This mechanism allows to detect the spin polarization of a half-filled p shell.

The paper is organized as follows. Section II describes the microscopic model, electronic structure, total spin, and the emission spectrum of the system of many electrons and a hole in a QD doped with a single Mn atom. Section III summarizes the results of the calculations of the emission spectra from nonmagnetic QDs as a function of the number of initial-state electrons, and discusses in detail the emission from a magnetic QD containing p-shell electrons, i.e., X^{2-} and X^{3-} complexes. In this section, we also compare the emission spectra of X-, X^--, X^{2-}-, and X^{3-}-Mn complexes and discuss the differences and similarities between them. At last, we discuss the effects of Mn position on the X^{2-}-Mn PL spectrum. Summary of the work is presented in Sec. IV.

II. MODEL

We model the confining potential of the QD in the effective-mass approximation as a quasi-two-dimensional isotropic

harmonic oscillator (HO).[38,39] Since the strain in the QDs results in the significant splitting between the light- ($\tau = \pm 1/2$) and heavy-hole ($\tau = \pm 3/2$) subbands,[40] we retain only heavy-holes in this calculations. We define the single-particle basis for electrons (hole) in terms of the eigenstates of the isotropic parabolic quantum dot with the characteristic frequency $\omega_{e(h)}$. The basis states are denoted by $|i\sigma\rangle$ for the electron and $|j\tau\rangle$ for the hole, where the complex index denotes a set of the HO quantum numbers $i = \{n,m\}$, while σ (τ) is a spin z projection of the particle. Each single-particle state has an angular momentum of $L_e = m - n$ for the electron and $L_h = n - m$ for the hole. The energies of these single-particle states are given by $E_i^{e(h)} = \omega_{e(h)}(n + m + 1)$.

We measure energy in units of the effective Rydberg, Ry* $= m^* e^4 / 2 \epsilon^2 \hbar^2$, and length in the units of the effective Bohr radius, $a_0^* = \epsilon \hbar^2 / m^* e^4$, where e is the electron charge, $\hbar$ is the reduced Planck constant, m^* is the effective mass of the electron, while ϵ is the dielectric constant of the material.

The Hamiltonian of the confined, interacting $N_e + 1$ electrons and a valence hole interacting with the spin of the magnetic impurity can be written in the second quantization language as[31,34]

$$
\begin{aligned}
H &= \sum_{i,\sigma} E_{i,\sigma}^e c_{i,\sigma}^\dagger c_{i,\sigma} + \frac{1}{2} \sum_{\substack{i,j,k,l \\ \sigma,\sigma'}} \langle i,j | V_{ee} | k,l \rangle c_{i,\sigma}^\dagger c_{j,\sigma'}^\dagger c_{k,\sigma'} c_{l,\sigma} \\
&\quad + \sum_{i,\tau} E_{i,\tau}^h h_{i,\tau}^\dagger h_{i,\tau} - \sum_{\substack{i,j,k,l \\ \sigma,\tau}} \langle i,j | V_{eh} | k,l \rangle c_{i,\sigma}^\dagger h_{j,\tau}^\dagger h_{k,\tau} c_{l,\sigma} \\
&\quad - \sum_{i,j} \frac{J_{i,j}^e(R)}{2} [(c_{i,\uparrow}^\dagger c_{j,\uparrow} - c_{i,\downarrow}^\dagger c_{j,\downarrow}) M_z + c_{i,\downarrow}^\dagger c_{j,\uparrow} M^+ \\
&\quad + c_{i,\uparrow}^\dagger c_{j,\downarrow} M^-] + \sum_{i,j} \frac{3 J_{i,j}^h(R)}{2} (h_{i,\Uparrow}^\dagger h_{j,\Uparrow} - h_{i,\Downarrow}^\dagger h_{j,\Downarrow}) M_z,
\end{aligned}
\tag{1}
$$

where $c_{i,\sigma}^\dagger$ ($h_{i,\tau}^\dagger$) creates an electron (hole) on the orbital i with spin σ (τ). The first two terms of the Hamiltonian are the electron kinetic energy and the electron-electron Coulomb interaction (e-e). The next two terms describe the hole kinetic energy and the Coulomb interaction between the hole and all electrons. The fifth term, describing the short-range electron-Mn (e-Mn) interaction,[24] consist of two types of terms. The first one is the Ising interaction, which conserves the spin of both the electron and the Mn. The second and third terms of the e-Mn Hamiltonian allow for the simultaneous flip of the electron and Mn spins in such a way as to conserve $M_z + \sigma$. The last term is the anisotropic heavy-hole-Mn spin interaction,[22,41] which describes a scattering of the hole from i to j single-particle states by a Mn ion at the position R. The e-Mn and hole-Mn (h-Mn) interaction is proportional to the $s(p)$-d exchange matrix elements, $J_{i,j}^{e(h)}(R) = J_C^{e(h)} \phi_i^*(R) \phi_j(R)$, where $\phi_i(R)$ is the value of the HO wave function at the position R, while $J_C^{e(h)} = 2 J_{s(p)-d}/d$. $J_{s(p)-d}$ is the bulk exchange contact interaction parameter, while d is the height of the QD. As $J_{i,j}^{e(h)}(R)$ depends on the position R of the Mn ion in the QD, by changing R one can control the strength of the e-Mn interaction.[24]

The many-particle wave function is expanded in the basis of the configurations of $N_e + 1$ electrons and a hole $|v_i\rangle = |i_{1\uparrow}, i_{2\uparrow}, \ldots, i_{N\uparrow}\rangle | j_{1\downarrow}, j_{2\downarrow}, \ldots, j_{N\downarrow}\rangle |k\rangle |M_z\rangle$, where $|j_{1\sigma}, j_{2\sigma}, \ldots, j_{N\sigma}\rangle = c_{j_1,\sigma}^\dagger c_{j_2,\sigma}^\dagger, \ldots, c_{j_{N_\sigma}}^\dagger |0\rangle$ is a state of N_σ electrons, each with spin σ, while $|k\rangle = h_{k,\tau}^\dagger |0\rangle$ is the hole state. $|M_z\rangle$ denotes all possible spin states of the Mn ion, $M_z = -5/2, \ldots, 5/2$, while $|0\rangle$ denotes the vacuum. The total number of electrons $N_e + 1 = N_\uparrow + N_\downarrow$, where $N_\uparrow$ and $N_\downarrow$ are the number of electrons with spin up and spin down, respectively. After recombination and emission of a photon, we are left with N_e electrons and the Mn ion. The final states of N_e electrons $|v_f\rangle$ are built in a similar way. The many-particle basis states are characterized by the total angular momentum $L = \sum_{i=1}^{N_e+1} L_e^i + L_h$ as well as an electron and hole spins $s_z = \sum_{i=1}^{N_e+1} \sigma_i$ and τ or $L = \sum_{i=1}^{N_e} L_e^i$ and $s_z = \sum_{i=1}^{N_e} \sigma_i$ for the initial and final states, respectively.

Having obtained the initial and final states, one can calculate the circularly polarized emission spectra from the Fermi's golden rule:

$$
E(\omega) = \sum_f P_i |\langle v_f | \mathcal{P} | v_i \rangle|^2 \delta(\mathcal{E}_i - \mathcal{E}_f - \omega),
\tag{2}
$$

where ω is the photon energy, while $\mathcal{E}_i$ and $\mathcal{E}_f$ are the energies of the initial and final states, respectively. The coefficient P_i is the probability of thermal occupation of the initial state $|v_i\rangle$, $P_i = \exp(-\mathcal{E}_i/kT)/P_{\text{SUM}}$, with $P_{\text{SUM}} = \sum_i \exp(-\mathcal{E}_i/kT)$. The interband polarization operator $\mathcal{P} = \sum_{kl} \langle k | l \rangle c_k h_l$ removes one electron-hole pair from the initial state. The optical selection rules[34] are defined by the overlap $\langle k | l \rangle$ between the electron and hole orbitals.

III. ELECTRONIC STRUCTURE AND EMISSION SPECTRA OF CHARGED MAGNETIC DOTS

In this section, we present the results of numerical calculation of the emission spectra of multiply charged QDs doped with a single Mn ion. Recent experiments and theory[18,42] indicate that in the CdTe quantum dots there are at least three confined single-particle shells, s, p, and d, and the presence of the d shell can give rise to new effects, such as the quantum interference (QI).[18] When Mn is in the center of the QD ($R = 0$), only those electrons that occupy the zero angular momentum orbitals are coupled with it. In the presence of three shells in the QD, there are two zero angular momentum orbitals, one in the s and one in the d shell.

The calculations are carried out with the following parameters: Ry* $= 12.11$ meV, $a_0^* = 5.61$ nm, for CdTe with the dielectric constant $\epsilon = 10.6$. The electron and hole effective masses are $m^* = 0.1 m_0$ and $m_h = 4 m^*$, respectively, with m_0 being the free-electron mass. The electron characteristic frequency $\omega_e = 1.98$ Ry* and $\omega_h = \omega_e/4$. The constant scaling the exchange contact interaction in the bulk CdTe for electrons is $J_{s-d} = 15$ meV nm^3, and for holes is $J_{p-d} = 60$ meV nm^3, while the height of the QD $d = 2$ nm.

As already mentioned, first we present the emission spectra for a nonmagnetic QD for $N_e = 0$ to 6. In the case of $N_e = 6$, both s and p shells of the QD are filled. After that, we investigate in detail the PL of X^{2-} and X^{3-} complex for the QD doped with a single Mn atom in its center. Lastly, we compare
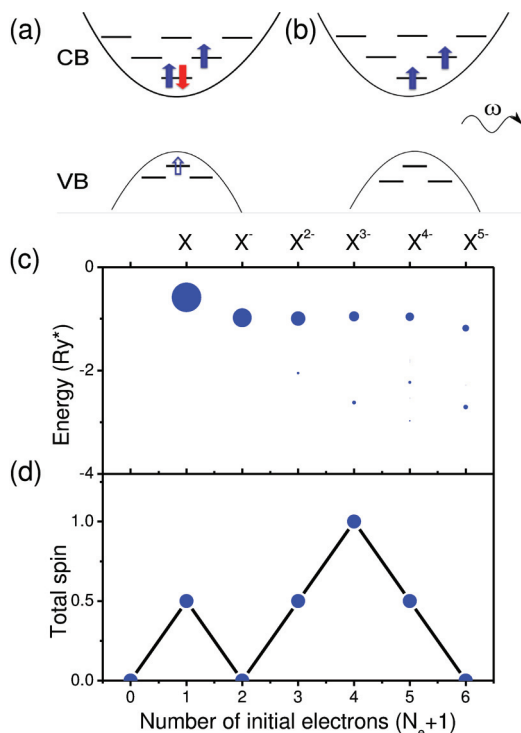
FIG. 1. (Color online) A schematic representation of (a) the ground state of an X^{2-} complex, formed by three electrons and a spin-up hole, and (b) the final state after recombination of electron-hole pair from the configuration (a). (c) Emission spectrum of a nonmagnetic QD calculated in the σ_+ polarization as a function of the number of electrons in the initial state. It is assumed that the probability P_i of occupation each of the degenerate initial states is equal. (d) Total spin of electrons in the ground state of the initial system as a function of the number of confined electrons.

the emission spectra from X, X^-, X^{2-}, and X^{3-} complexes confined in a magnetic QD and discuss their features.

A. Emission from a nonmagnetic charged quantum dot

Figure 1(a) schematically shows a ground state of the X^{2-} complex, composed of three electrons in the conduction band (CB) and a hole in the valence band (VB). Two electrons and the hole occupy the s shell, while the third electron is in the p shell. After the electron-hole recombination from the X^{2-} complex, the final state is formed by two electrons in the CB and a photon with energy ω, as shown in Fig. 1(b). The remaining two electrons can be either in a triplet or in a singlet spin configuration, which have the same kinetic energy but are split by the e-e exchange Coulomb interaction.[34]

Figure 1(c) shows the evolution of the recombination spectrum in σ_+ polarization as a function of the number of electrons in the initial (photoexcited) state. The area of the circles is proportional to the intensity of individual transitions. The emission is symmetric with respect to the hole spin, so the σ_- polarization spectrum is exactly the same.

For doubly (X^{2-}) and higher-charged exciton states, the emission peak splits into two or more. The splitting in the emission spectra originates from the splitting of the final state as discussed above and in Ref. 34. From the emission spectra of

nonmagnetic QDs, one can not draw conclusion about the spin of N_e electrons left after the electron-hole pair recombination.

Figure 1(d) illustrates the total electron spin of the initial ground state as a function of number of electron in this state. The QD is filled obeying the QD Hund's rule.[34] Until each shell is half-filled, subsequent electrons are added with the same spin, increasing the total spin of this shell. After the half-filling is reached, electrons are added with opposite spin, which results in the spin zero of a completely filled shell. As the p shell is being filled, the maximum spin is reached when there are four electrons in the QD, while in the presence of six electrons, both s and p shells are filled, and the spin of electrons is equal to zero.

B. X-Mn and X^--Mn complexes

The emission spectra of both the exciton X and negatively charged exciton X^- interacting with the spin of the Mn ion have been described previously.[12,18,20] Here we briefly summarize these results.

The ground state (GS) of the exciton-Mn system can be approximated by the configuration in which the electron and the hole occupy their respective s shell. The final states left after the electron-hole pair recombination are the degenerate states $|M_z\rangle$ of Mn. Thus the emission spectrum from X-Mn complex consists of six emission lines (one for each M_z). The splitting between these lines corresponds directly to the splittings between X-Mn states, approximated by $1/2(3J_{ss}^h + J_{ss}^e)$ in the symmetric QDs.[12] Since the h-Mn exchange constant J_{ss}^h is four times greater than the e-Mn exchange constant J_{ss}^e, the splittings are dominated by the h-Mn interaction.[12,18]

The GS of a negatively charged exciton X^- interacting with Mn consists of two electrons and one hole, all occupying the single-particle s shell. The two electrons are in the singlet state, which prevents them from interacting with Mn. X^- interacts with Mn only through the h-Mn Ising Hamiltonian, which splits the otherwise degenerate X^--Mn into six levels similarly to the X-Mn case. However, in contrast to the X-Mn complex, there are two final states of the one e-Mn system with one electron on the s shell interacting with the Mn ion. These two e-Mn states have $J = S + M = 2$ or 3 and are split by the e-Mn interaction. Since the emission from the initial state with $M_z = 5/2$ to the final state with $J = 2$ is forbidden, the emission spectrum of the X^--Mn has eleven lines arranged into six groups.[20] The emission spectra of the X-Mn and X^--Mn complexes will be shown in greater detail later on.

C. X^{-2}-Mn complex

Here we present the emission spectra from X^{2-}-Mn complex confined in our magnetic QD with a single Mn ion in its center. We begin with a detailed description of the electronic structure of both initial and final states and then discuss the calculated emission spectrum.

1. Initial state

The ground state of the X^{-2} complex confined in a nonmagnetic QD can be approximated by the lowest-energy configuration shown schematically in Fig. 1(a). The X^{-2} GS is fourfold degenerate: twice with respect to the spin of the
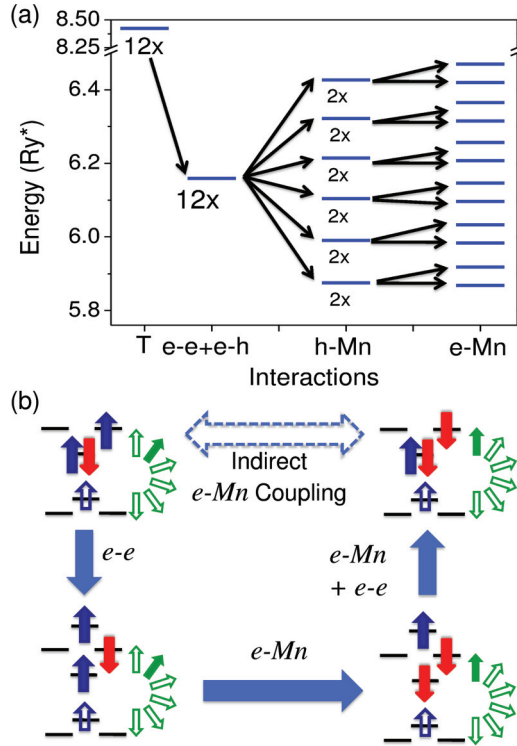
FIG. 2. (Color online) (a) The ground-state energy of the X^{2-}-Mn system as a function of interactions (subsequent terms added towards the right-hand side of the panel). The degeneracy of the energy levels is marked. The splitting in the ground state caused by e-Mn interaction is not to scale. (b) The coupling scheme between the $|X^{2-}, s_z = 1/2\rangle$ and $|X^{2-}, s_z = -1/2\rangle$ configurations. Filled arrows indicate the direct coupling, while the dashed arrow indicates an indirect coupling.

electron in the p shell and twice with respect to its angular momentum ($L = \pm 1$). Since the total angular momentum L is a good quantum number, the analysis will be carried out in the $L = 1$ subspace. The double degeneracy of the GS of X^{2-} complex due to the spin persists even in the presence of e-e and e-h interactions. The two main configurations of the X^{2-} complex are $|X^{2-}, s_z = 1/2\rangle = c_{s\uparrow}^+ c_{p\uparrow}^+ c_{s\downarrow}^+ h_{s\Uparrow}^+ |0\rangle$ and $|X^{2-}, s_z = -1/2\rangle = c_{s\uparrow}^+ c_{s\downarrow}^+ c_{p\downarrow}^+ h_{s\Uparrow}^+ |0\rangle$. These two states do not interact with each other since they have different spin projections s_z. In a QD with three confined single-particle shells, one can construct 198 different configurations of X^{2-} complex with $L = 1$, which interact either with $|X^{2-}, s_z = 1/2\rangle$ or with $|X^{2-}, s_z = -1/2\rangle$ via e-e and e-h Coulomb interactions. In a magnetic QD with Mn in its center, the angular momentum is conserved, and the total number of the X^{2-}-Mn configurations increases $(2M + 1) = 6$ times, reaching 1188 configurations in the $L = 1$ subspace.

Figure 2(a) shows the evolution of the X^{2-}-Mn low-lying energy spectrum with inclusion of interactions. The first column shows calculations with only kinetic energy T, second after we include e-e and e-h Coulomb interactions, third with h-Mn interaction added, and finally fourth includes e-Mn interaction. In the absence of any interactions, the GS is twelvefold degenerate, twice due to electron spin and six times due to Mn spin orientations. This degeneracy does not change after inclusion of the e-e and e-h Coulomb

interactions, however the energy of the complex decreases. After addition of the h-Mn Ising-type interaction, Eq. (1), the ground state of the X^{2-}-Mn complex splits into six doubly degenerate levels. Since none of the $|X^{2-}, s_z = 1/2\rangle$ and $|X^{2-}, s_z = -1/2\rangle$ configurations interact directly with the Mn via e-Mn interaction, $\langle X^{2-}, s_z = 1/2 | H_{\text{e-Mn}} | X^{2-}, s_z = 1/2\rangle = \langle X^{2-}, s_z = -1/2 | H_{\text{e-Mn}} | X^{2-}, s_z = -1/2\rangle = 0$, one expects no change in the energy spectra of the X^{2-}-Mn complex after inclusion of the e-Mn interaction as in Eq. (1). However, addition of the e-Mn interaction leads to further splitting of the X^{2-}-Mn energy levels as shown in Fig. 2(a). Since the e-Mn coupling is smaller than the h-Mn coupling, the resulting splitting is magnified out of scale in order to visualize the effect. The origin of this splitting is in the indirect coupling between the p-shell electrons and Mn, mediated by e-e Coulomb interaction.

Figure 2(b) shows the coupling scheme among seemingly noninteracting configurations of X^{2-} complex and Mn ion. In order to simplify the discussion, we focus only on the splitting caused by the e-Mn interaction. The filled arrows indicate a direct coupling between the X^{2-}-Mn configurations, while the dashed arrow represents an indirect coupling.

Let us start form the $|X^{2-}, s_z = 1/2\rangle \otimes |M_z\rangle$ configuration, see Fig. 2(b) top left. This configuration is coupled via e-e Coulomb interaction with an excited configuration (with the same s_z and M_z) with a spin-down electron in the p shell, and two unpaired electrons in the s and d shells. The e-Mn interaction can flip the spin of the spin-up electron in the s shell with simultaneous flip of the Mn spin to $M_z + 1$, as illustrated in the bottom of Fig. 2(b). This excited state with $s_z = -1/2$ and $M_z + 1$ is coupled with the $|X^{2-}, s_z = -1/2\rangle \otimes |M_z + 1\rangle$ via the e-e Coulomb interaction as well as the e-Mn interaction ($J_{sd}(0) \neq 0$).

One can replace the coupling scheme between $|X^{2-}, s_z = 1/2\rangle \otimes |M_z\rangle$ and $|X^{2-}, s_z = -1/2\rangle \otimes |M_z + 1\rangle$ configurations presented in Fig. 2(b) by filled arrows with a single dashed arrow, representing the indirect coupling. Effectively, one can look at this coupling as that of the p-shell electrons to a Mn ion, mediated by e-e and e-Mn interactions.

2. Final state

The final state left after the electron-hole recombination from the X^{2-}-Mn complex is composed of one electron in the s shell and one in the p shell, as illustrated in Fig. 1(b). This state has the same total angular momentum as the initial state, namely, $L = 1$. The remaining electrons can be in a triplet state with total spin $S = 1$, or in a singlet state with $S = 0$. These states have the same kinetic energy, therefore in the absence of any interaction they are 24 times degenerate, four times due to electron spin and six times due to Mn spin.

Figure 3(a) shows the evolution of the energy of X^{2-} final states with the inclusion of different types of interactions. The e-e Coulomb interaction splits the triplet and the singlet states. The triplet is 18 times degenerate, while the singlet is sixfold degenerate. Addition of the e-Mn interaction leads to the splitting of the triplet state into three levels with eight-, six-, and fourfold degeneracy. The triplet state of the pair of electrons on the s and p shell experiences the same kind of splitting as a particle with $S = 1$ interacting with Mn
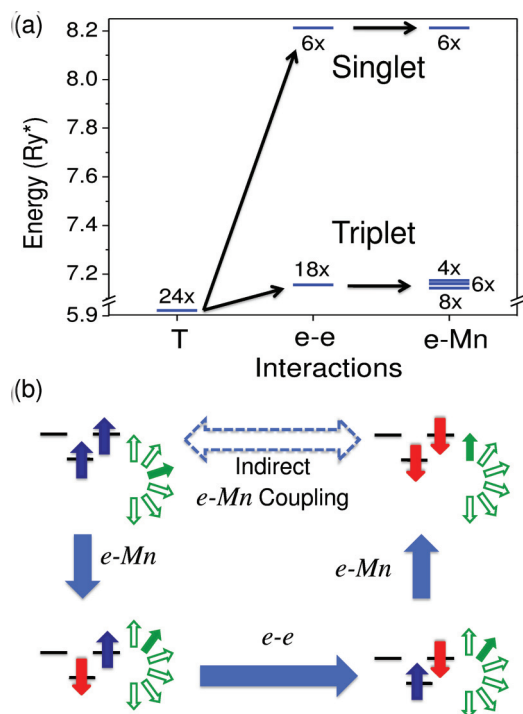
FIG. 3. (Color online) (a) Evolution of the final-state energy as a function of interactions, with marked degeneracy of the energy levels. (b) The coupling scheme between the final-state configurations. Types of arrows have the same meaning as in Fig. 2(b).
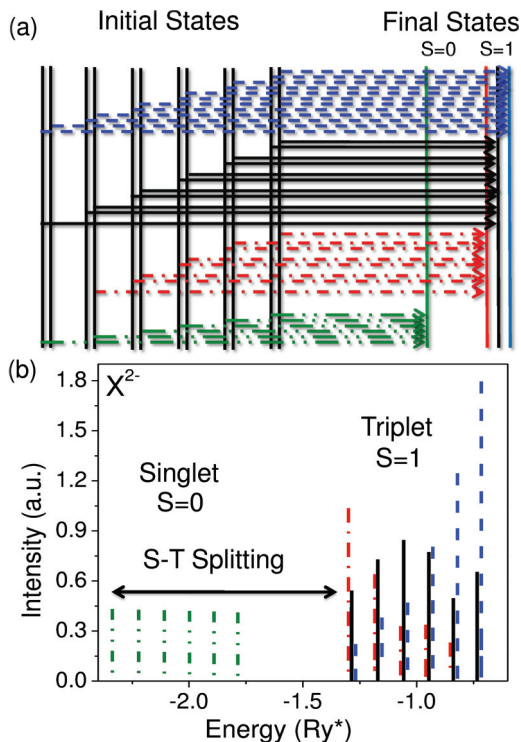

FIG. 4. (Color online) (a) The energy levels of initial and final states with allowed transitions between them indicated by the arrows. The dashed, solid, and dashed-dot arrows denote the transitions to the $S = 1$ electron states, while the dashed-double-dotted arrow denotes the transitions to the $S = 0$ final electron states. (b) Emission spectrum of X^{2-}-Mn complex calculated in the σ_+ polarization as a function of the photon energy.

via ferromagnetic interactions. At the same time, the singlet remains six times degenerate.

To understand the fine structure of the triplet state, let us analyze how the electrons interact with Mn. Figure 3(b) shows the coupling scheme between two pairs of s-p electrons: $|s_z = 1\rangle \otimes |M_z\rangle$ and $|s_z = -1\rangle \otimes |M_z + 2\rangle$ in the presence of the Mn ion. Again, the filled arrows indicate a direct coupling between the configurations, while the dashed arrow indicates an indirect coupling. Let us start from the configuration $|s_z = 1\rangle \otimes |M_z\rangle$, Fig. 3(b), top left. The e-Mn spin-flip interaction couples it with the configuration with $s_z = 0$ and $M_z + 1$, where the electron with the spin $s_z = -1/2$ is on the s shell. This configuration is coupled by the e-e Coulomb interaction with a configuration with $s_z = 0$ and $M_z + 1$, but the spin down electron occupying the p shell. Again, the e-Mn interaction couples the former configuration with the $|s_z = -1\rangle \otimes |M_z + 2\rangle$, through the e-Mn spin-flip process. Effectively, the coupling scheme shown by the filled arrows can be replaced by the dashed arrow, representing the indirect coupling between configurations $|s_z = 1\rangle \otimes |M_z\rangle$ and $|s_z = -1\rangle \otimes |M_z + 2\rangle$. From this coupling scheme, one can conclude that indeed a pair of s-p electrons interacts with Mn ion in the same way as a spin $S = 1$ particle, with three possible spin projections $S_z = -1, 0, 1$, changing the spin of Mn from $|M_z\rangle$ to $|M_z + 2\rangle$, with simultaneous change of its spin from $S_z = 1$ to $S_z = -1$. The difference is that in a spin Hamiltonian both spins ($S = 1$ and $M_z = 5/2$) interact directly, while in our model, the coupling with the p-shell electron is indirect.

3. Emission spectrum

Having obtained the X^{2-} initial and final eigenvalues and eigenstates, we calculate the emission spectrum of X^{2-}-Mn complex. The spectrum in the σ^+ polarization is calculated at temperature in which a thermal population of the twelve lowest X^{2-}-Mn states is equal [$P_i = 1$ in Eq. (2)]. The σ^+ polarized light is emitted due to the recombination of the spin-up hole and a spin-down electron from the initial X^{2-}-Mn state. Both total angular momentum of the electronic state as well as M_z are conserved in the recombination process.

Figure 4(a) schematically shows the energy levels of both initial and final states. The dashed, solid, and dashed-dotted arrows indicate the optically active transition from all twelve initial states to the triplet final states, split into three levels with degeneracy eight, six, and four. The dashed-double-dotted arrows present six optically active transitions from the initial states with electron spin $s_z = -1/2$ to the sixfold degenerate singlet state.

The emission spectrum from the X^{2-}-Mn complex is shown in Fig. 4(b), with the colors and styles of lines corresponding to the styles of arrows in Fig. 4(a). The emission spectrum consists of two groups of transitions [as in a QD without Mn in Fig. 1(c)]: the lower lying transitions (six dashed-double-dotted lines) correspond to the transition to the final state with the two electrons in a singlet state ($S = 0$), while the higher-lying group corresponds to the transitions to their triplet state ($S = 1$).

Let us start the discussion by analyzing the lower-energy part of the spectrum presented by dashed-double-dotted peaks. Since the final state—in this case an electron singlet—is degenerate, the splitting between the emission lines corresponds to the splitting between the initial states due to the hole-Mn interaction. One could expect that each of the lines is in fact a doublet, with the small splitting between them due to the e-e and e-Mn interactions, however, only one of them is bright: only states with $s_z = -1/2$ can have an electron singlet as a final state. The existence of the *six* lines in the emission confirms the previous hypothesis of the s-p electron pair behavior as a $S = 0$ particle.

In the higher-energy part of the emission spectra [see Fig. 4(b)], the transitions to the final states of electrons in a triplet states are presented. This part of emission spectra consists of six groups of peaks split by the h-Mn interaction in the initial state. Five of the main peaks are then further split into three due to the e-e and e-Mn-induced splitting in the final state and correspond to different final states. The highest-energy main peak is split into two, since the transition from the highest energy state of the X^{2-}-Mn complex to the fourfold-degenerate final state is dark. Therefore, by looking at the energy difference between two consecutive peaks, within the same main peak, i.e., the solid and dashed-dot peaks, one can obtain the effective splitting of the final state, which depends on e-e and e-Mn interactions. Each of these peaks can be further split, reflecting the e-Mn induced splitting in the initial state giving total of 31 optically active transitions, however this splitting is not visible on the scale of Fig. 4(b).

D. X^{3-}-Mn complex

The simplest system allowing to study the behavior of electrons in a half-filled shell is the X^{3-} complex. In the GS of this complex, the two electrons in the p shell are in a triplet state $S = 1$, which makes them a good candidate to interact with the Mn spin. Indeed, as we have shown previously, there exists an effective interaction between the p-shell and the Mn spin mediated by the e-e Coulomb interactions. Here we describe the electronic properties of the initial and final states of the X^{3-} complex and its emission spectrum.

1. Initial state

The GS of the X^{3-} is composed of four electrons and one hole. As previously, we focus only on one subspace, with the hole spin projection $\tau = 3/2$. The lowest-energy configurations of the X^{3-} complex have total angular momentum equal to zero, and are fourfold degenerate in the absence of e-e Coulomb interactions. The degeneracy is due to the four possible spin configurations of the two unpaired electrons in the p shell: they can be either spin polarized ($s_z = \pm 1$) or with $s_z = 0$, creating either a singlet or a triplet state.

The total number of the X^{3-}-Mn configurations with the angular momentum $L = 0$ and $\tau = 3/2$ in a QD confining three single-particle shells is 2664. The excited configurations of the X^{3-}-Mn complex play an important role in mediating the interactions between the p-shell electrons and Mn. Therefore the X^{3-} complex allows us to study the behavior of $S = 1$ and 0 spins interacting indirectly with Mn.
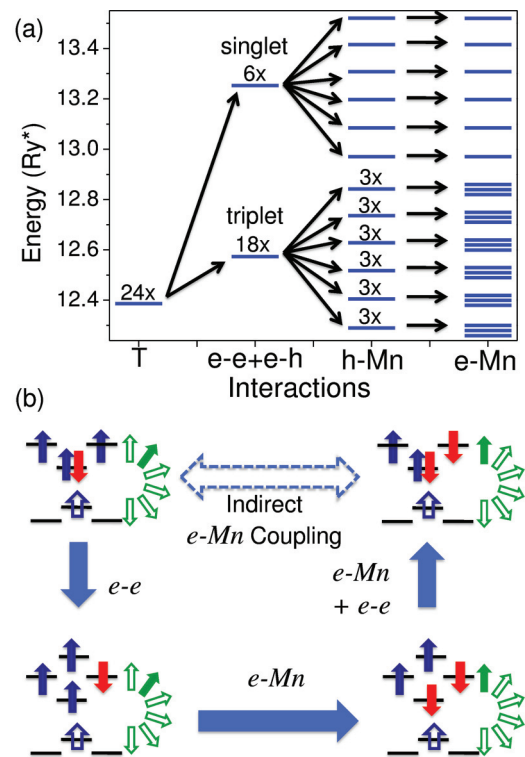

FIG. 5. (Color online) (a) The ground-state energy of X^{3-}-Mn complex as function of interactions, with marked degeneracy of the energy levels. The splitting in the GS caused by e-Mn interaction is out of scale. (b) The coupling scheme between X^{3-}-Mn configurations with different s_z. Types of arrows have the same meaning as in Fig. 2(b).

Figure 5(a) shows the evolution of the GS energy as we add the interactions. With inclusion of the Coulomb interactions between the carriers, the 24-fold degenerate X^{3-}-Mn GS splits into two states: a lower-lying triplet-Mn (18-fold degenerate) and a singlet-Mn (sixfold degenerate). The h-Mn interaction breaks the Mn symmetry and splits both of these manifolds into six levels. Each of the six triplet-Mn levels is still threefold degenerate. This degeneracy is lifted by e-Mn interaction. This takes place only in the presence of the e-e Coulomb interaction in the QDs containing at least three shells and it is another proof that both of the p electrons are coupled indirectly with the Mn ion. The splitting of singlet-Mn state remains unchanged, but its energy is lowered in relation to the system without e-Mn interaction. As the e-Mn splitting is smaller than the h-Mn splitting, it is out of scale in Fig. 5(a).

Figure 5(b) shows the coupling scheme between X^{3-}-Mn configurations with different s_z. The configuration of X^{3-}-Mn with two spin-up electrons in the p shell and the Mn spin M_z is coupled by e-e Coulomb interactions with an excited configuration (with the same M_z) in which the spin-down electron is scattered to the p shell and the spin-up electron is scattered to the d shell [as shown in the bottom-left panel of Fig. 5(b)]. The e-Mn interaction can flip the spin of the electron occupying the s shell, with a simultaneous increase of the Mn spin by one (to the state with $M_z + 1$). Now, this configuration is coupled via e-e Coulomb interactions with a low-energy X^{3-}-Mn configuration in which there is a spin-up

and spin-down electron in the p shell and the Mn spin is in the state $M_z + 1$. Therefore all initial states forming the GS manifold are indirectly coupled via e-e and e-Mn interactions, as shown by the dashed arrow. This coupling breaks the triplet degeneracy and can be again treated as one induced by an indirect coupling between two p-shell electrons and the Mn ion.

2. Final state

The final state, left over after recombination of the spin down electron with the spin up hole from the X^{3-} complex, is an *excited state* of the three electrons system (with $L = 0$). It is formed by one electron in the s shell and two in the p shell. However, since the configurations with two electrons in the s shell and one in the d shell have the same kinetic energy as the configurations mentioned before, they are strongly coupled by the e-e Coulomb interaction.

Figure 6(a) shows the coupling scheme between four three-electron-Mn (3e-Mn) configurations with the same kinetic energy but with different s_z. The coupling mechanism between the configurations is the same as that explained in previous sections.

Figure 6(b) illustrates how the energies of the 3e-Mn system evolve as interaction terms are added. In the absence of any interactions, all of the considered configurations have the same energy. This energy level is 60-fold degenerate, ten due to electron configurations times six Mn spin orientation. Addition of the e-e Coulomb interaction splits the energy of the 3e-Mn complex into four levels, with degeneracy 24, 12, 12, 12,
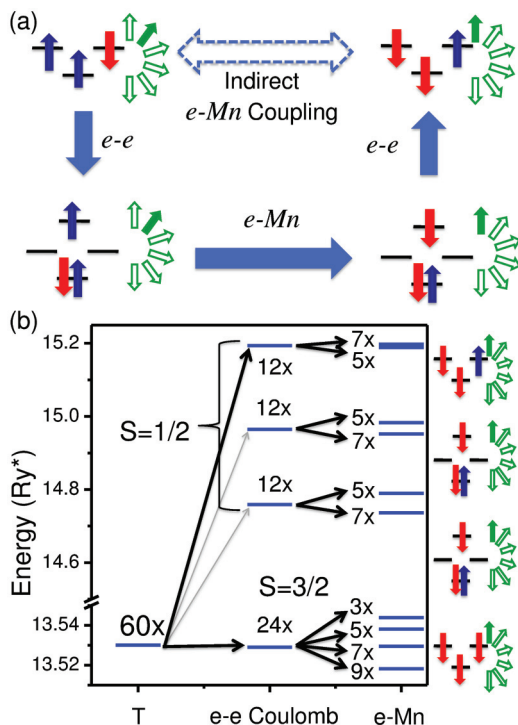

FIG. 6. (Color online) (a) The coupling scheme between the three-electron-Mn configurations with different s_z. Types of arrows have the same meaning as in Fig. 2(b). (b) Evolution of the final-state energy with various interaction terms, the numbers indicate the degeneracy of the energy levels.

respectively. The lowest-energy electron state has total spin $S = 3/2$, while all higher energy levels correspond to $S = 1/2$. It is important to notice that the two intermediate $S = 1/2$ states are not final states of the X^{3-} complex recombination in a QD with or without Mn. It is so because they are built by the configurations with two electrons in the s shell and the third electron in the d shell mixed with the configurations with one electron on the s shell and a pair of electrons occupying the p shell in a singlet state. At the same time, the lowest and higher energy states are formed mostly by configurations with only one electron in the s shell and two in the p shell, allowing them to be final states in the recombination of the X^{3-}(-Mn) complex.

In the presence of the e-Mn interaction, the $S = 3/2$ level splits into four states and each of the $S = 1/2$ levels into two. We observe that the $S = 3/2$ and two first $S = 1/2$ three-electron states are ferromagnetically coupled with Mn, since the degeneracy of levels (related to total electron-Mn spin) decreases as a function of energy. The ordering of states is different in the case of highest $S = 1/2$ state, which is antiferromagnetically coupled with Mn.

3. Emission spectrum

Here we investigate the emission from the equally populated initial states of the X^{3-}-Mn complex with $S = 1$ [18 lowest energy levels in Fig. 5(a)]. The emission spectra from the X^{3-}-Mn complex consist of two main groups of peaks corresponding to optical transitions from the initial states to the $S = 3/2$ and the highest of $S = 1/2$ final states, in the way resembling the emission from X^{3-} in nonmagnetic QD [see Fig. 1(b)]. These two types of transitions will be analyzed separately.

Figure 7(a) shows the X^{3-}-Mn initial and final energy levels, with the dashed arrows denoting the transitions to the highest two final states with $S = 1/2$. The emission spectrum from X^{3-}-Mn complex to these final states consists of six groups of peaks and it is shown in Fig. 7(b). The splitting into main six groups is caused by the h-Mn interaction in the initial state, while the splitting into two peaks in each group is due to the e-Mn interaction in the final state. The effects of the splitting of the initial state induced by the e-Mn interaction are not visible in this figure, but they cause further splittings of emission lines. Figure 8(a) shows the X^{3-}-Mn initial and final energy levels, with the solid arrows representing optical transitions from all initial states to four final states with $S = 3/2$ (differentiated by the color).

In the high-energy part of the X^{3-}-Mn emission spectrum, Fig. 8(b), there are also six main groups of peaks originating from the splitting of the initial states due to the h-Mn interaction. Each of these groups is further split by the e-Mn interaction in both the final and initial states. To observe these splittings, the details of the emission from the first three energy levels of the initial state to the four final states with $S = 3/2$ are shown in the inset. It consists of nine emission lines (three transitions are dark), arranged into four groups, each corresponding to a different final state. The splitting between these four groups corresponds to the strength of e-Mn interaction in the final state, while the splitting within each group is due to the indirect e-Mn interaction in the initial state.
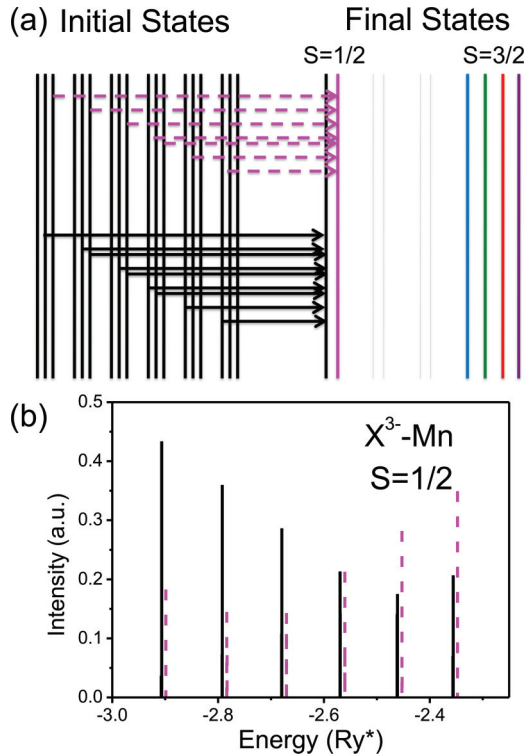
FIG. 7. (Color online) (a) Schematic representation of the X^{3-}-Mn initial and final states, with the allowed transitions to the final states with $S = 1/2$ indicated by the dashed arrows. (b) The low-energy X^{3-}-Mn emission spectrum in σ_+ polarization. The styles of emission lines correspond to the styles of arrows (a).

The e-Mn-induced splitting in the final state is larger than that in the initial state, because the final-state configuration has an electron in an open s shell directly interacting with Mn, while in the initial state, the interaction between p-shell electrons and Mn is mediated by e-e Coulomb interactions.

E. Comparison between emission spectra of different complexes

Now we analyze the evolution of the emission spectrum for the right circularly polarized light as the number of excess electron N_e confined in the QD is increased. In Fig. 9(a), we show the comparison between the emission spectra of X-Mn, X^--Mn, and the high-energy parts of the emission spectra of X^{2-}-Mn, and X^{3-}-Mn complexes. The emission spectra of these complexes are shown as a function of the number N_e of extra electrons in a QD in Fig. 9(b), where the low-energy peak is clearly marked in red. Its energy is almost the same for $X-$, X^{2-}, and X^{3-}-Mn, and it is much lower than the low-energy peak for X-Mn. This corresponds to the similar plateau as is visible in the emission of a nonmagnetic charged QD[34,37] [see Fig. 1(c)].

Figure 9(c) shows the evolution of the low-energy emission lines with the number of excess electrons N_e. For the X-Mn complex, there is only one emission line, since there is only one final state of the electron-hole recombination, being the state of Mn with $M_z = -5/2$. The emission from the lowest state of X^--Mn complex consists of two lines with the splitting between them corresponding to the final-
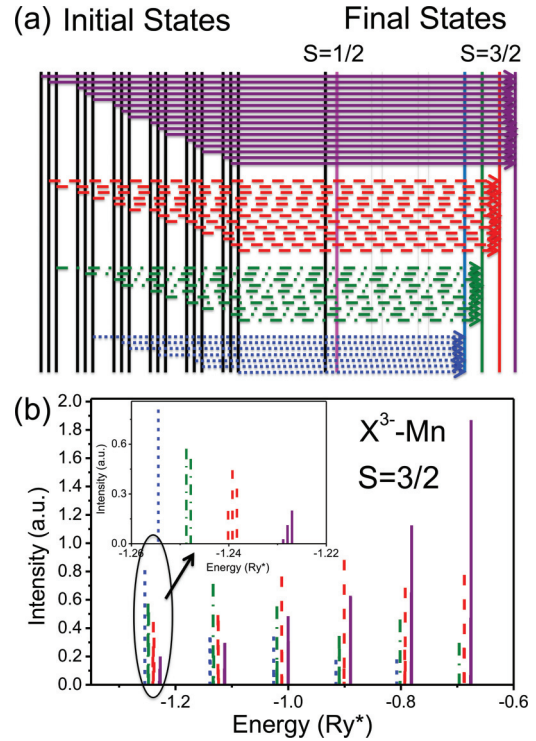

FIG. 8. (Color online) (a) Schematic representation of the X^{3-}-Mn initial and final states, and the allowed transitions from all initial states to the $S = 3/2$ final states indicated by the arrows. (b) High-energy part of the X^{3-}-Mn emission spectrum in σ_+ polarization. The styles of emission lines correspond to the styles of arrows in (a). The inset shows the emission from the first group of three initial states to all final states with $S = 3/2$.

state splitting (electron-Mn complex creating state with total angular momentum $J = 2$ or $J = 3$). In the case of the X^{2-}-Mn complex with $S = 1$, there are three final states of the two-electron system, all of them triplets. Again, the splitting between the emission lines can be translated into the splitting between final states. The lowest-energy emission spectrum of the X^{3-}-Mn complex with $S = 3/2$ consists of four groups of levels, with the splitting between them reflecting the splitting of the four final states of three electrons with $S = 3/2$ as described in the previous section. Each of these groups exhibits a fine structure related to the fine structure of the initial state.

F. Effects of Mn in an off-center position

When Mn is positioned away from the dot center, the cylindrical symmetry of the dot is broken and the total angular momentum L is no longer a good quantum number. As a result, the states with finite angular momenta, e.g., $L = \pm 1$, are coupled by Mn-induced scattering of the carriers, which opens additional gaps in the spectrum. Moreover, carriers occupying QD orbitals with non-zero angular momentum, e.g., p orbitals, interact directly with Mn. Figures 10(a) and 10(b) allows to compare the emission spectra from X^{2-}-Mn complex confined in the QD with Mn ion in the center $R = (0,0)$ (a) and at position $R = (0.3 l_0, 0)$ away from the center (b). Indeed, in Fig. 10(b), one can observe additional peaks that arise from the removal of degeneracy of energy levels, which for a rotationally symmetric dot were orbitally degenerate, in
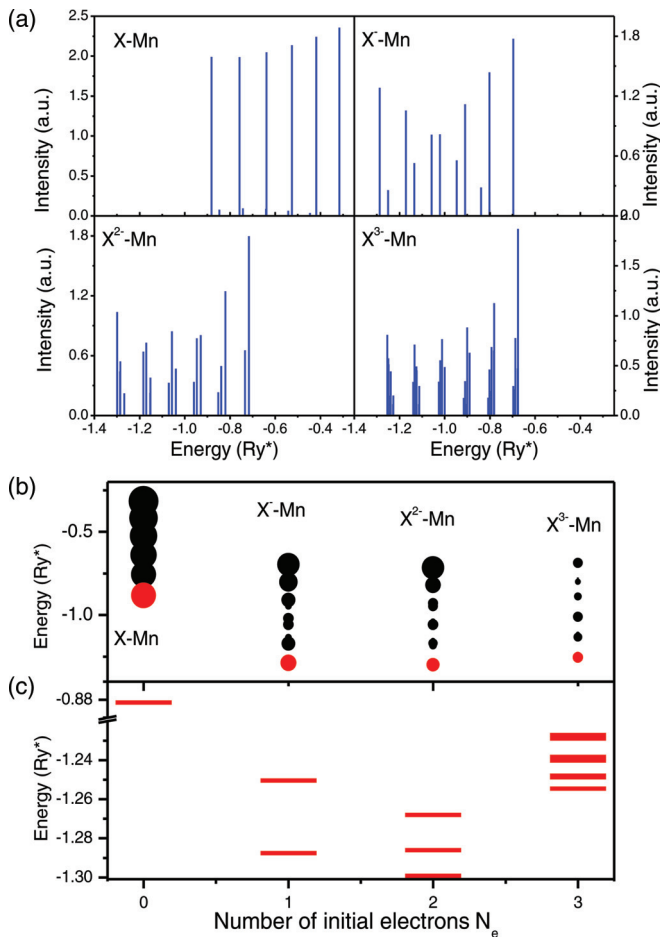
FIG. 9. (Color online) (a) Emission spectrum of X-Mn, X^--Mn complexes, and high-energy part of the spectrum of X^{2-}-Mn and X^{3-}-Mn complexes. (b) Emission spectra from (a) as a function of the number of electrons in the initial state. (c) Close-up of the lowest-energy emission lines as a function of the number of electrons in the initial state with clearly visible multiplicity of lines.

this case states with $L = \pm 1$. Shifting Mn to a more off-center position leads to significant changes in the emission spectrum, as discussed in Refs. 26 and 43.

In previous sections, we have demonstrated that the measure of the strength of the indirect p-electron-Mn interactions is given by the splitting of the six groups of the emission lines in the X^{2-}-Mn spectrum, and this in turn is determined by the splitting of the final state of the emission. This allows to assess the relative importance of the indirect component of that interaction, which is the only coupling mechanism for the impurity in the center of the QD, compared to the direct p-electron-Mn interaction, which is present when the impurity is shifted off-center. In Fig. 10(c), the evolution of the energies of the 2e-Mn complex as the Mn is displaced is presented. Figure 10(c) (left) shows the evolution of the 2e-Mn spectrum as a function of Mn position capturing all direct and indirect terms, while in Figure 10(c) (right) the direct interactions is turned off, artificially setting $J_{pp} = 0$. In Fig. 10(c) (left), the three sets of lines split as the impurity is shifted as due to symmetry breaking. However, apart from that, the splitting of 2e-Mn complex (the large gaps) is of the same order in both cases until the position of Mn exceeds $R \approx (0.6l_0, 0)$. We
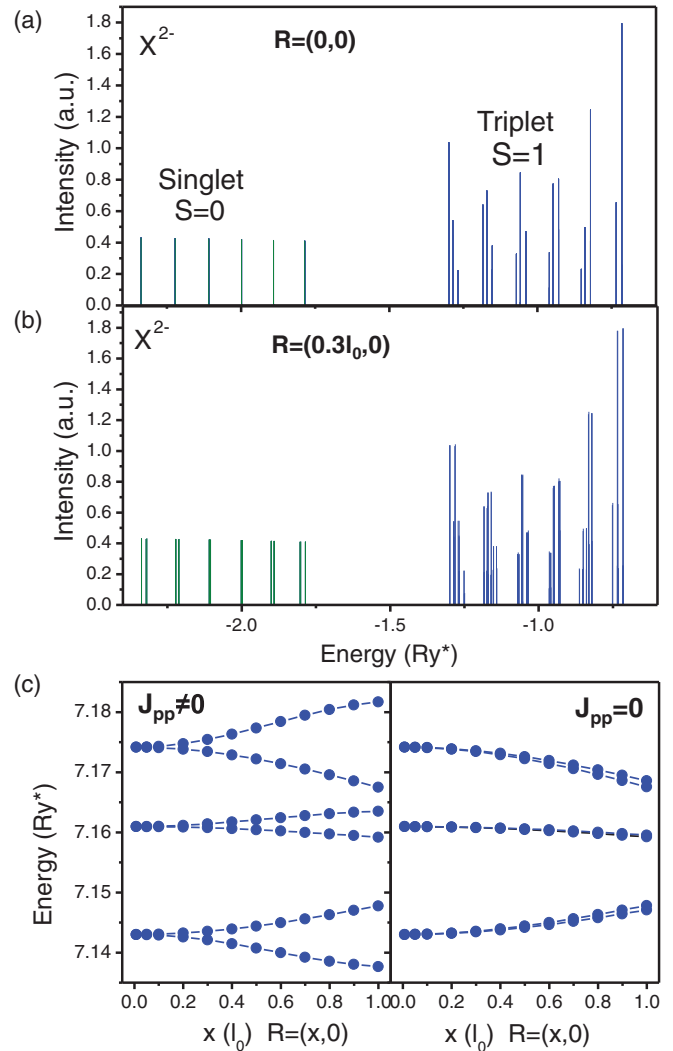

FIG. 10. (Color online) Emission spectrum of X^{2-}-Mn complex when Mn is in the center $R = (0,0)$ (a) or at position $R = (0.3l_0, 0)$ (b). (c) Comparison between the splitting of 2e-Mn complex in the presence $J_{pp} \neq 0$ (left) and absence $J_{pp} = 0$ (right) of direct p-electron-Mn interaction.

conclude that the indirect interaction is dominating the direct one over very broad range of the Mn position in the QD, and as such should not be ignored.

IV. SUMMARY

In summary, we presented a microscopic theory of the optical properties of self-assembled quantum dots doped with a single magnetic (Mn) impurity containing a controlled number of electrons N_e. The total spin of the electron complex is controlled by the population of electronic shells: it is zero for closed shells and maximal for half-filled shells. We show that even though electrons may occupy electronic states that are not coupled directly with Mn, there exists an indirect coupling mediated by electron-electron interactions. This coupling allows for the detection of electron spin and verification of Hund's rules in self-assembled quantum dots from emission spectra. We have shown that the indirect interaction between p electrons and Mn ion is an important effect even when

Mn is shifted away from the center of the quantum dot, and dominates over the direct interaction over a broad range of Mn positions. The details and a complete analysis of this e-Mn coupling mediated by e-e Coulomb interaction is a subject of a further study.[44]

[1] P. Hawrylak, M. Grabowski, and J. J. Quinn, Phys. Rev. B **44**, 13082 (1991).

[2] S. Loth, K. von Bergmann, M. Ternes, A. F. Otte, C. P. Lutz, and A. J. Heinrich, Nat. Phys. **6**, 340 (2010).

[3] S. T. Ochsenbein, Y. Feng, K. M. Whitaker, E. Badaeva, W. K. Liu, X. Li, and D. R. Gamelin, Nat. Nanotechnol. **4**, 681 (2009).

[4] D. A. Bussian, S. A. Crooker, M. Yin, M. Brynda, A. L. Efros, and V. I. Klimov, Nat. Mat. **8**, 35 (2009).

[5] T. Dietl, Nat. Mater. **9**, 965 (2010).

[6] P. Hawrylak, in *The Physics of Diluted Magnetic Semiconductors*, edited by J. Gaj and J. Kossut, Springer Series in Materials Science (Springer-Verlag, Berlin, 2011).

[7] P. M. Koenraad and M. E. Flatté, Nat. Mater. **10**, 91 (2011).

[8] *Semiconductor Quantum Bits*, edited by F. Henneberger and O. Benson (Pan Stanford Publishing, Singapore, 2008).

[9] C-Y. Hsieh, Y. P. Shim. M. Korkusinski, and P. Hawrylak, Rep. Prog. Phys. **75**, 114501 (2012).

[10] P. Hawrylak and M. Korkusinski, in *Single Quantum Dots: Fundamentals, Applications, and New Concepts*, edited by P. Michler, Topics in Applied Physics Vol. 90, (Springer-Verlag, Berlin, 2003).

[11] G. Kioseoglou, M. Yasar, C. H. Li, M. Korkusinski, M. Diaz-Avila, A. T. Hanbicki, P. Hawrylak, A. Petrou, and B. T. Jonker, Phys. Rev. Lett. **101**, 227203 (2008).

[12] L. Besombes, Y. Leger, L. Maingault, D. Ferrand, H. Mariette, and J. Cibert, Phys. Rev. Lett. **93**, 207403 (2004).

[13] A. Hundt, J. Puls, and F. Henneberger, Phys. Rev. B **69**, 121309 (2004).

[14] L. Besombes, Y. Leger, L. Maingault, D. Ferrand, H. Mariette, and J. Cibert, Phys. Rev. B **71**, 161307 (2005).

[15] A. Kudelski, A. Lemaitre, A. Miard, P. Voisin, T. C. M. Graham, R. J. Warburton, and O. Krebs, Phys. Rev. Lett. **99**, 247209 (2007).

[16] M. Goryca, T. Kazimierczuk, M. Nawrocki, A. Golnik, J. A. Gaj, P. Kossacki, P. Wojnar, and G. Karczewski, Phys. Rev. Lett. **103**, 087401 (2009).

[17] C. Le Gall, R. S. Kolodka, C. L. Cao, H. Boukari, H. Mariette, J. Fernandez-Rossier, and L. Besombes, Phys. Rev. B **81**, 245315 (2010).

[18] A. H. Trojnar, M. Korkusinski, E. S. Kadantsev, P. Hawrylak, M. Goryca, T. Kazimierczuk, P. Kossacki, P. Wojnar, and M. Potemski, Phys. Rev. Lett. **107**, 207403 (2011).

[19] L. Besombes, C. L. Cao, S. Jamet, H. Boukari, and J. Fernandez-Rossier, Phys. Rev. B **86**, 165306 (2012).

[20] Y. Leger, L. Besombes, J. Fernandez-Rossier, L. Maingault, and H. Mariette, Phys. Rev. Lett. **97**, 107401 (2006).

[21] A. L. Efros, M. Rosen, and E. I. Rashba, Phys. Rev. Lett. **87**, 206601 (2001).

[22] A. O. Govorov, Phys. Rev. B **70**, 035321 (2004).

[23] A. O. Govorov and A. V. Kalameitsev, Phys. Rev. B **71**, 035338 (2005).

[24] F. Qu and P. Hawrylak, Phys. Rev. Lett. **95**, 217206 (2005).

[25] F. Qu and P. Hawrylak, Phys. Rev. Lett. **96**, 157201 (2006).

[26] J. Fernandez-Rossier, Phys. Rev. B **73**, 045301 (2006).

[27] N. T. T. Nguyen and F. M. Peeters, Phys. Rev. B **78**, 245311 (2008).

[28] D. E. Reiter, T. Kuhn, and V. M. Axt, Phys. Rev. Lett. **102**, 177403 (2009).

[29] R. Oszwaldowski, I. Zutic, and A. G. Petukhov, Phys. Rev. Lett. **106**, 177201 (2011).

[30] J. Fernandez-Rossier and R. Aguado, Phys. Rev. Lett. **98**, 106805 (2007).

[31] S.-J. Cheng and P. Hawrylak, Europhys. Lett. **81**, 37005 (2008).

[32] A. H. Trojnar, M. Korkusinski, M. Potemski, and P. Hawrylak, Phys. Rev. B **85**, 165415 (2012).

[33] A. L. Gazoto, M. J. S. P. Brasil, F. Iikawa, J. A. Brum, E. Ribeiro, Y. A. Danilov, O. V. Vikhrova, and B. N. Zvonkov, Appl. Phys. Lett. **98**, 251901 (2011).

[34] A. Wojs and P. Hawrylak, Phys. Rev. B **55**, 13066 (1997).

[35] G. A. Narvaez and P. Hawrylak, Phys. Rev. B **61**, 13753 (2000).

[36] M. Ediger, K. Karrai, A. Badolato, P. M. Petroff, and R. J. Warburton, Phys. Stat. Sol. (c) **3**, 3806 (2006).

[37] D. Dalacu, M. E. Reimer, S. Frederick, D. Kim, J. Lapointe, P. J. Poole, G. C. Aers, R. L. Williams, W. R. McKinnon, M. Korkusinski, and P. Hawrylak, Laser Photon. Rev. **4**, 283 (2010).

[38] P. Hawrylak, Phys. Rev. Lett. **71**, 3347 (1993).

[39] A. Wojs and P. Hawrylak, Phys. Rev. B **53**, 10841 (1996).

[40] E. S. Kadantsev, M. Zielinski, M. Korkusinski, and P. Hawrylak, J. Appl. Phys **107**, 104315 (2010).

[41] Y. Leger, L. Besombes, L. Maingault, D. Ferrand, and H. Mariette, Phys. Rev. B **72**, 241309 (2005).

[42] A. H. Trojnar, M. Korkusinski, U. C. Mendes, M. Goryca, M. Koperski, T. Smolenski, P. Kossacki, P. Wojnar, and P. Hawrylak, Phys. Rev. B **87**, 205311 (2013).

[43] Y. Leger, L. Besombes, L. Maingault, D. Ferrand, and H. Mariette, Phys. Rev. Lett. **95**, 047403 (2005).

[44] U. C. Mendes, M. Korkusinski, and P. Hawrylak (unpublished).